Hindawi Publishing Corporation
Advances in Materials Science and Engineering
Volume 2013, Article ID 374080, 8 pages
http://dx.doi.org/10.1155/2013/374080

Research Article

Physical Properties and Selective CO Oxidation of Coprecipitated CuO/CeO_2 Catalysts Depending on the CuO in the Samples

Akkarat Wongkaew,[1] Wichai Kongsi,[2,3] and Pichet Limsuwan[2,3]

[1] *Department of Chemical Engineering, Faculty of Engineering, Burapha University, Chonburi 20131, Thailand*
[2] *Department of Physics, Faculty of Science, King Mongkut's University of Technology Thonburi, Bangkok 10140, Thailand*
[3] *Thailand Center of Excellence in Physics, CHE, Ministry of Education, Bangkok 10400, Thailand*

Correspondence should be addressed to Akkarat Wongkaew; akkarat@buu.ac.th and Pichet Limsuwan; opticslaser@yahoo.com

Received 19 March 2013; Revised 1 July 2013; Accepted 19 July 2013

Academic Editor: Markku Leskela

This paper investigates the effects of CuO contents in the CuO-CeO_2 catalysts to the variation in physical properties of CuO/CeO_2 catalysts and correlates them to their catalytic activities on selective CO oxidation. The characteristic of crystallites were revealed by X-ray diffraction, and their morphological developments were examined with TEM, SEM, and BET methods. Catalytic performance of catalysts was investigated in the temperature range of 90–240°C. The results showed that the catalyst was optimized at CuO loading of 20 wt.%. This was due to the high dispersion of CuO, high specific surface area, small crystallite sizes, and low degree of CuO agglomeration. Complete CO conversion with near 100% selectivity was achieved at a temperature below 120°C. The optimal performance was seen as a balance between CuO content and dispersion observed with growth, morphology, and agglomeration of nanostructures.

1. Introduction

The generation of clean electrochemical hydrogen energy via proton exchange membrane fuel cells (PEMFCs) has attracted wide interests for stationary and mobile applications with high efficiency, high power density, and rapid startup. A multistep process requires for producing hydrogen on board usually accomplished by reform of hydrocarbons or methanol, followed by high and low temperature water gas shift reaction (WGSR) [1–8]. Typical effluents from such a process contain 45–75% H_2, 5–10% H_2O, 10–20% CO_2, and a considerably high 0.5–2% CO, which is known to poison the Pt-based fuel cell anode if exists over 100–10 ppm [6–11]. Preferential oxidation of carbon monoxide (CO-PROX) is being considered by many researchers as the simplest and most cost effective method for removing CO [1–8, 12–14]. The PROXs catalysts should possess high activity and selectivity towards CO, wide operating temperature window, high tolerance to the presence of CO_2 and H_2O in the feed stream, and stability in time.

Binary CuO-ZnO and ternary CuO-ZnO-Al_2O_3 mixed oxide catalysts have been widely employed commercially for the WGSR. Unfortunately, the problems for applying CuO-ZnO catalysts under these conditions are pertain to poor thermal stability and the pyrophoricity of the material [10]. Efforts then have been spent on the development of catalysts for the CO-PROX reaction, such as the noble metal-based catalysts (Pt, Pd, Ru, and Rh), gold-based catalyst, and transition metal based catalysts (Co, Cu, and Mn) [15, 16]. The platinum-group metal catalysts suffer from poor selectivity at 150–200°C; moreover, the presence of H_2O and CO_2 in the feed stream significantly reduces the lifetime of gold-based catalysts [7, 16, 17]. The low cost CuO-CeO_2 catalysts are remarkably more selective than Pt-based catalysts at low operating temperatures [1, 6, 8, 13, 18]. This enhancement occurs in vicinity of the interfacial perimeter which begins with the generation of oxygen vacancies in the support and as the result provokes higher oxygen mobility and diffusion from the lattice to the interface [8, 19]. The ceria-based catalysts have high oxygen storage capacity (OSC), strong

interaction with active metal, and easily change between Ce^{3+} and Ce^{4+} by synergism [12, 14, 20]. Catalytic properties are intimately associated with the support and structure, and recently well-dispersed copper oxide patches over ceria nanoparticles had been spectroscopically rationalized [1]. The redox behavior of cerium oxide can be modified by incorporation of other elements to form mixed oxides with high mobility of lattice oxygen, high oxygen storage capacity, well-dispersed and good adsorption, and reducibility of Cu. The introduced elements, in many reports, formed solid solutions with CeO lattice [8, 15, 16, 21, 22].

The characteristic properties that affect the catalytic performance are usually observed in terms of surface area, particle size, dispersion of the active metals, and structural defects such as oxygen vacancies [7]. These properties depend strongly on synthesis methods, pretreatment conditions, and presence of dopants [12, 22, 23]. Several preparation methods such as urea-nitrate combustion, sol-gel, and coprecipitation have been described [12, 21]. Recently, advanced preparation techniques reported were the hydrothermal and the inverse configuration of CeO_2/CuO [18]. Regardless of catalysts preparation methods, CuO loading certainly plays an important role in the structure forming of the catalysts. The composition affects greatly the formation of various nanostructures. There have been a number of reports on the effect of CuO loading on the catalytic performance of the CuO/CeO_2 catalyst. However, most of the works were presented with CuO loading within specific range, for example, <15 wt.% [17].

In this work, the variation in physical properties and CO oxidation performances of coprecipitated CuO/CeO_2 catalysts were investigated over whole range of CuO loadings. The activity and selectivity of the catalysts were discussed and correlated with their characterizations results obtained from XRD, TEM, SEM, and BET measurements. The changes on morphology of nanostructures and agglomeration of structures observed with CuO loadings could assist us in identifying influential factors in term of synergistic effect on performance of the catalyst.

2. Experimental

2.1. Catalyst Preparation. Catalysts of various CuO/CeO_2 weight ratios were prepared by coprecipitation method. For each weight ratio, the proper amount of $Cu(NO_3)_2{\cdot}3H_2O$ (BDH) and $Ce(NO_3)_3{\cdot}6H_2O$ (Aldrich) was dissolved separately in 400 mL of deionized water. Then, 100 mL each of these two salt solutions were mixed well using a magnetic stirrer. NH_4OH solution (Richer Chemicals) of 1 M was slowly added into the previous solution under continuous stirring. The precipitate was observed at pH 9. The solution was continuously stirred for 30 min. After stirring, the precipitate was washed with deionized water several times to remove excess ions. The cleaned precipitate was dried at 110°C for 24 h and then calcined at 500°C for 10 h. The obtained powder was ground and sieved to mesh sizes of 80–100. The weight ratios of CuO to CeO_2 investigated in this work were 10/90, 20/80, 40/60, 60/40, 80/20, and 90/10. The catalyst will thereafter be referred to by the CuO weight %; that is, 20% CuO represents the catalyst containing 20% of CuO and 80% of CeO_2 by weight.

2.2. Structural Characterization

2.2.1. X-Ray Diffraction, TEM, and SEM Measurements. The crystalline structure of the catalysts was characterized by X-ray diffraction (XRD) technique. Powder XRD patterns were recorded at room temperature using a Bruker D8 advance powder diffractometer equipped with a CuK_α and a nickel filter. The working voltage was 40 kV, and the current was 40 mA. The diffraction intensity was measured in the 2θ range of 20°–75° with a step of 0.02° in a scan time of 8 s. The X-ray spectra were identified by comparison with JCPDS files. The average crystallite size of CuO and CeO_2 catalysts was calculated using Scherrer's equation from the X-ray line broadening of the (111) diffraction peak of CeO_2 and CuO.

A TEM (JEOL JSM-2100) equipped with an EDX system operated at 200 kV was used to determine the characteristics of nanostructures as well as observing the dispersion of the 20% CuO catalyst. The SEM images (JEOL JSM-6510) were taken at 5 kV for all CuO loadings for observing agglomeration.

2.2.2. BET Surface Areas. BET measurement was used to determine the surface area and pore size of CuO/CeO_2 catalysts. The measurement was carried out with adsorption-desorption isotherms of liquid N_2 using Autosorption-1 C from Quantachrome. Approximately 100 mg of calcined catalyst was placed in a quartz reactor. Before measuring, the catalyst was heated at 200°C for 0.5 h under N_2 gas purging as a pretreatment. The BET surface area and pore size of all CuO/CeO_2 catalysts with different weight ratios were calculated at N_2 adsorption-desorption isotherms with P/Po between 0.05 and 0.35.

2.3. Catalytic Activity Test. The activity tests were carried out in a fixed-bed reactor (4 mm ID) at atmospheric pressure. For each test, 80 mg of catalyst was loaded inside the reactor on top of quartz wool. The reaction temperature inside the reactor was measured by a *K*-type thermocouple placed on the top of the catalyst bed, and the reactor was controlled by a temperature controller (OMEGA: CN3251). For CO oxidation, the gas feed contained 1% CO, 1% O_2, and He balance. For selective CO oxidation, the gas feed contained 1% CO, 1% O_2, 60% H_2, and He balance (without H_2O) and 1% CO, 1% O_2, 60% H_2, 2.8% H_2O, and He balance (with H_2O). The total gas flow rate of the reaction mixture was controlled to 80 $cm^3\ min^{-1}$ or space velocity of 60,000 $cm^3\ g^{-1}\ h^{-1}$. The compositions of products and reactants were analyzed by a gas chromatograph (Varian CP-3800) equipped with TCD. An ice cooled water condenser was used to remove water from the gas streams before entering GC.

The CO conversion was obtained by comparing the CO concentration at the bypass line and the outlet stream from the reactor. Selectivity to CO oxidation was defined as the ratio of oxygen consumed by CO oxidation to the total oxygen consumption (obtained by subtracting the O_2

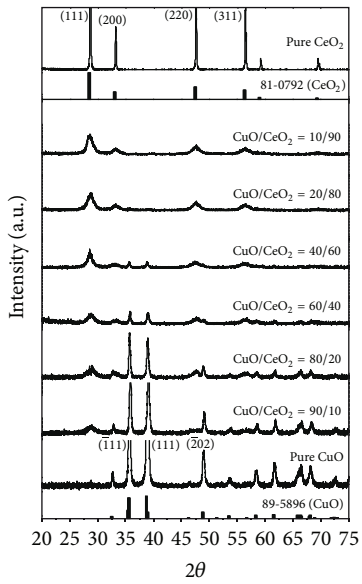

Figure 1: XRD patterns of CuO/CeO_2 catalysts for various CuO loadings.

concentration at the reactor outlet from the O_2 concentration in the feed). The amount of O_2 not used in CO oxidation reaction was assumed to oxidize H_2. Importantly, there was no methane formation observed under reaction conditions performed in this study. The selectivity can be expressed as the follows:

$$\text{selectivity to CO oxidation} = \frac{0.5\left[[\text{CO}]_{\text{in}} - [\text{CO}]_{\text{out}}\right]}{[\text{O}_2]_{\text{in}} - [\text{O}_2]_{\text{out}}} \times 100. \quad (1)$$

3. Results and Discussion

3.1. Structural Characterization

3.1.1. XRD and TEM Results. Figure 1 shows the XRD patterns of catalysts for various CuO/CeO_2 weight ratios; all of catalysts were synthesized under the same conditions. The dominant diffraction peaks of CeO_2 correspond to the (111), (200), (220), and (311) planes of the cubic phase of fluorite CeO_2 in Joint Committee on Powder Diffraction Standard (JCPDS) file number 081–0792. The monoclinic phase CuO crystalline in the ($\bar{1}11$), (111), and ($\bar{2}02$) planes according to the JCPDS file number 089–5896 is not detected for catalysts containing less than 20 wt.% CuO.

The presence of the CuO phases for catalysts containing less than 20 wt.% CuO was confirmed with TEM results in Figure 2. The TEM micrographs of the 20% CuO catalyst show agglomeration of nanoparticles with the primary crystallite size of CuO estimated at 6.0 nm. The spotty rings of SAED image in Figure 2(b) confirm the polycrystalline nature of the catalyst. The *d*-spacing of 0.91 nm in Figure 2(c) of HRTEM image corresponds to monoclinic phase CuO in the XRD results. Careful observation on Figure 2(c), it appears the agglomeration of randomly oriented epitaxially interfaced crystallites and the presence of amorphous structures. Due to the significantly lower surface energy of CeO_2 than any forms of the copper oxides, the result would theoretically be an encapsulation of the copper species or clusters by the cerium dioxide. This is observable in the figure; a few loosely-packed CuO clusters are forming an agglomerated particle. This suggests that the CuO phases are well dispersed over CeO_2 support [21, 24].

Table 1: Physical properties of the catalysts.

Sample	S_{BET}	Average pore	Average crystallite size (nm)	
(wt.%)	(m^2/g)	size (nm)	CuO (111)	CeO_2 (111)
CuO/CeO_2 = 0/100	40.6	—	—	17.1
CuO/CeO_2 = 10/90	105.7	4.2	—	11.02
CuO/CeO_2 = 20/80	109.2	4.4	5.9	10.4
CuO/CeO_2 = 40/60	106.7	5.8	8.84	10.4
CuO/CeO_2 = 60/40	73.6	7.8	10.1	9.5
CuO/CeO_2 = 80/20	30.5	12.4	15.7	8.7
CuO/CeO_2 = 90/10	12.5	—	17.7	—
CuO/CeO_2 = 100/0	64.9	—	20.2	—

The average crystallite sizes of CeO_2 and CuO, calculated from the CeO_2(111) peak and CuO(111) peak using Sherrer's equation, are reported in Table 1. The crystallite size of pure CeO_2 is 17.1 nm, and it is reduced rapidly to 11.02 and 10.4 nm when CuO contents are 10 and 20 wt.%, respectively. The crystallite size of CeO_2, thereafter, remains close to 10 nm over increasing CuO loading. This result indicates that the presence of Cu(II) ions hinders the crystalline growth of cerianite [25]. The crystallite size of CuO was also observed decreasing after the introduction of CeO_2. The pure CuO crystallite is 20.2 nm, and it is reduced to 5.9 nm for the 20% CuO catalyst. This is well established in bimetallic systems that the less reducible metal inhibits the aggregation of the easily reduced metal [22] and hence as a result the well dispersion of CuO onto ceria support for the catalyst. Similar effects were observed for inverse configuration CeO_2/CuO (high CuO content) in which larger CuO particles act as the support for ceria [12].

3.1.2. BET Surface Area and SEM Micrographs. The BET surface area and average pore size of these catalysts are listed in Table 1. It is seen that the BET surface areas of pure CuO and pure CeO_2 are clearly smaller than those of mixed oxides CuO/CeO_2 catalysts. The high surface areas (109–106 m^2/g) were obtained with the catalyst with CuO contents of 20 and 40 wt.%, respectively. Increase the CuO content to 80 wt.% strongly reduces the surface area to 30.5 m^2/g.

The morphology development of the catalyst is demonstrated by a sequence of SEM micrographs in Figure 3 (SEM micrographs of some CuO contents are not presented). The SEM results revealed agglomeration of particles. While the pure CeO_2 nanoparticles packed into regularly polyhedra of a few micrometers large, pure CuO aggregated into almost round particles with a wide range of particle size distributions.

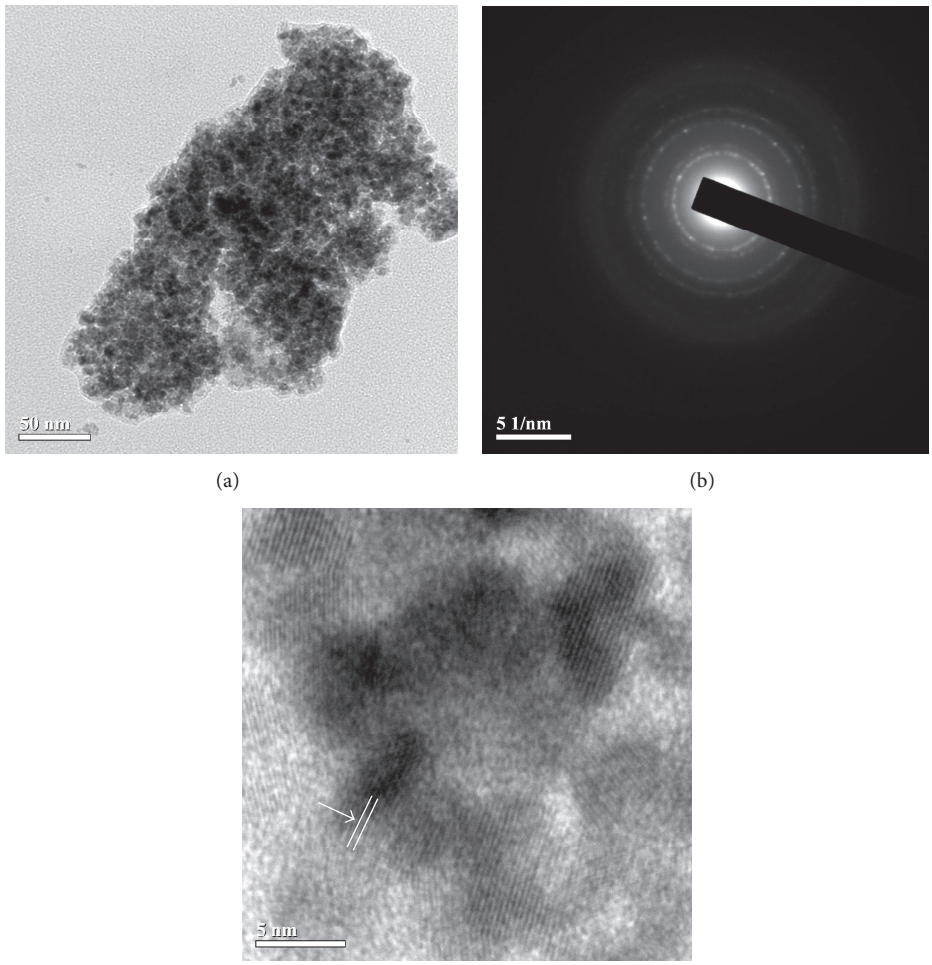

(a) (b)

(c)

Figure 2: TEM results of 20% CuO/CeO_2: (a) typical TEM image, (b) SAED, and (c) HRTEM images.

For the catalysts of CuO content between 10 and 20 wt.%, a uniform morphology with narrow particle size distribution was observed. This indicates the effectiveness of CeO_2 support in anchoring and dispersing of CuO, and consequently the catalyst exhibits a low degree of CuO agglomeration. The aggregation of mixed nanoparticles generates voids between particles. The low degree of CuO agglomeration provides a larger interface area and together with a small CuO crystallite is responsible for high surface area (~109.2 m^2/g) of the catalyst.

For higher contents of CuO (>40 wt.%), crystallites were agglomerated into larger particles with increasing CuO content. Some researchers had revealed the composite distribution of the catalysts over several ranges of CuO content. Such a result that is the EFTEM elementary maps of Ce, Cu, and O particles had been shown with indiscernible of CeO_2 and CuO composites [24]. This suggested a composite of cluster with its morphology described with the TEM results. A constant Cu/Ce ratio was also found in the particles of different sizes with the catalyst synthesized by Jobbagy et al. [25].

At very high copper contents (>80 wt.%), the XRD results present with strong crystallinity of CuO. Due to the low amount of CeO_2 to adequately disperse and oxidize the active metal, CuO was agglomerated into larger bulk CuO. This bulk CuO is the third form of copper in the composite oxides which can be examined by XRD; however, it makes little contribution to catalytic activity.

3.2. CO Oxidation Activity. The catalytic performance of the CuO/CeO_2 catalysts was firstly investigated on CO oxidation with the feeding gases containing 1% CO, 1% O_2, and He balance. The CO conversion results for the catalysts of different CuO contents (wt.%) are presented along with the performance of the pure oxides in Figure 4.

Pure CeO_2 shows constantly low activity over the temperature range, while the CO conversion for the pure CuO rises sharply after 130°C and reaches 70% conversion at around 190°C. The catalyst of 10% CuO loading lowers the 50% CO conversion (T50) temperature by almost 80°C. The remarkable increase of catalytic activity at low temperature

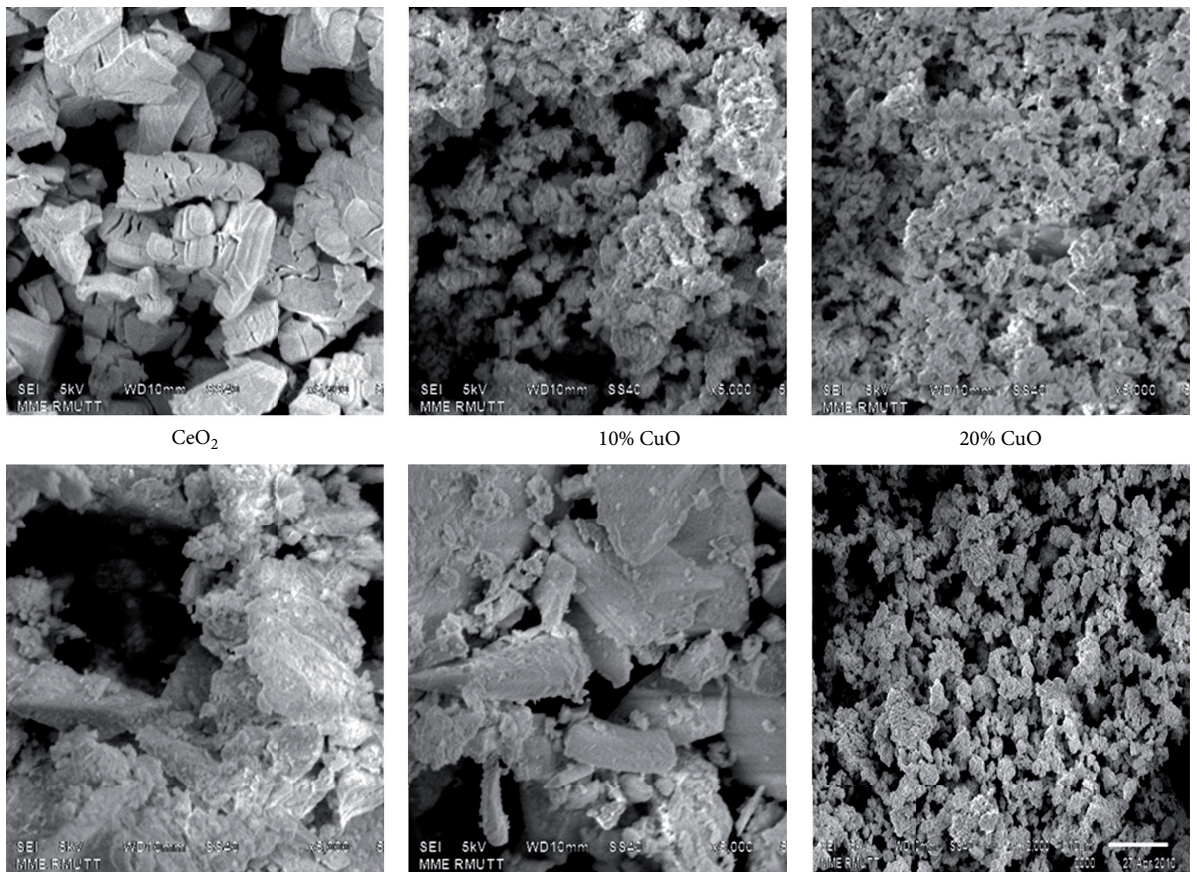

Figure 3: SEM micrographs of the catalysts with the percentage numbers below each picture indicated the level of CuO loading by wt.%.

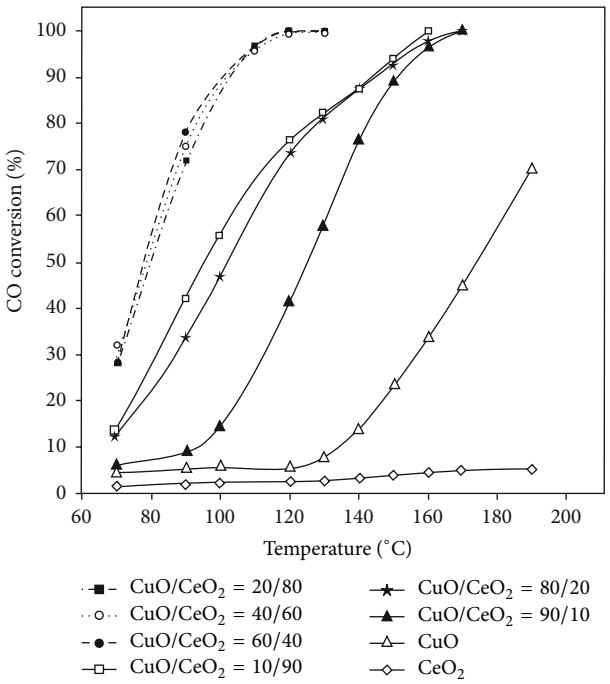

Figure 4: CO oxidation performances of CuO/CeO_2 catalysts for various weight ratios with their pure oxides are also shown. Feed composition (v/v): 1% CO, 1% O_2, and 98% He.

of the catalyst is well known and extensively reported as the synergetic effects. The low activity group of catalysts is seen with 10, 80, and 90 wt.% of CuO content. The sluggish activities of the catalysts are result from different effects and can clearly be observed in Table 1.

The 10% CuO catalyst possesses with high specific surface area and small CuO crystallite size, but its adverse characteristic is the larger CeO_2 crystallite size of (11.02 nm) and as a result lowers surface oxygen storage capability. The catalysts with 80% and 90% CuO content suffered directly from the low specific surface areas in addition to the large CuO crystallite sizes [7, 26]. Furthermore, the aggregation of crystallites to form a larger copper particle reduces the interface area and resulting in the weakening of the metal-support interaction [7, 27].

The high activity group of catalysts (CuO loading of 20, 40, and 60 wt%) can reach the full CO oxidation at temperature below 120°C. Considering the CuO loading for this group (20–60 wt.%), the development of cluster structures and agglomeration into larger particles was previously discussed with SEM and TEM results with increasing CuO content. An optimal number of CuO crystallites agglomerated into a nanostructured composite particle, referred to by Ayastuy et al. [21] as the number of CuO crystallites per particle, will enable the CeO_2 particles to more effectively supply surface oxygen for the CO oxidation and in close interaction as the

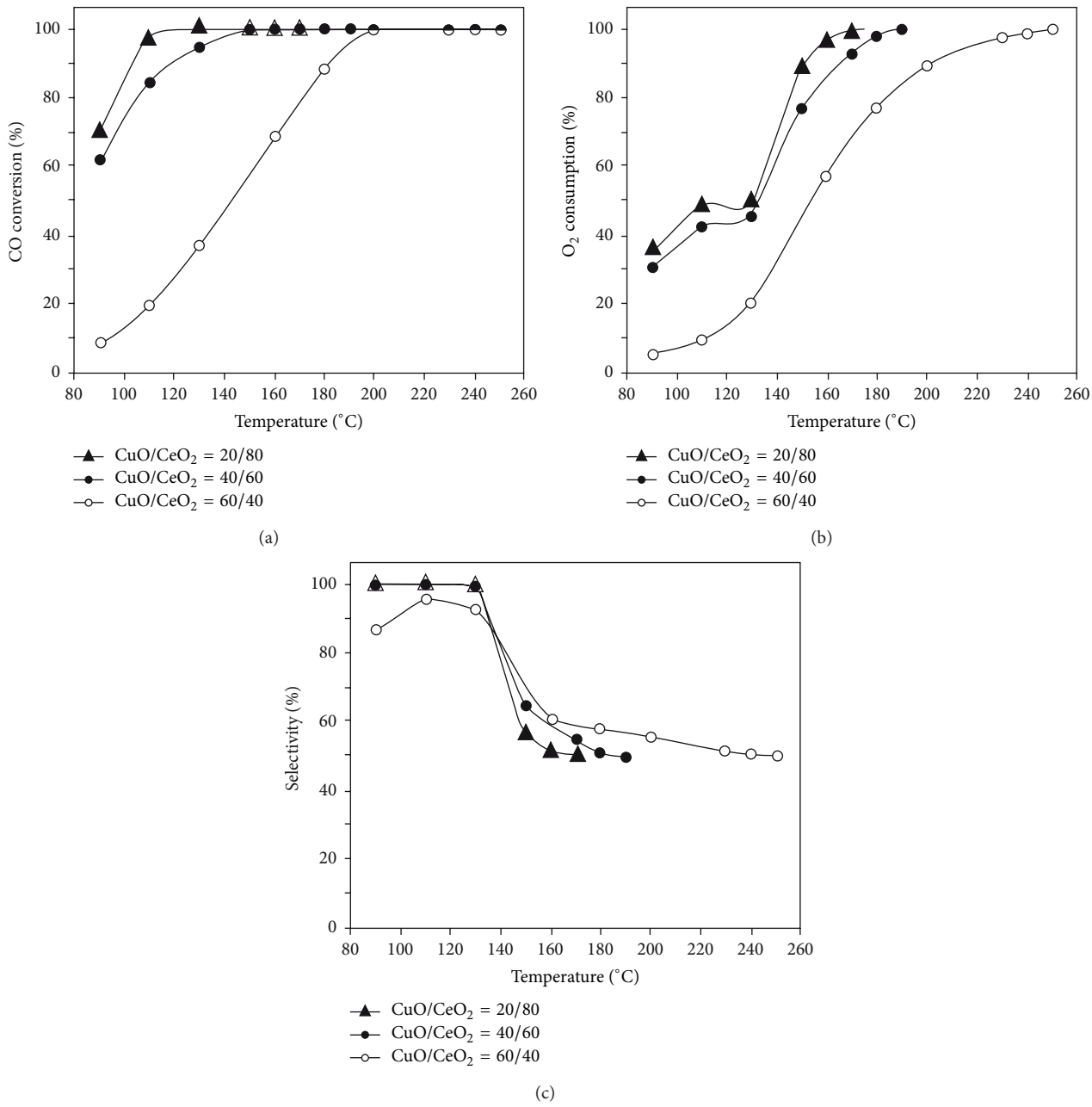

Figure 5: Selective CO oxidation performances of CuO/CeO_2 catalysts of various weight ratios: (a) CO conversion, (b) O_2 consumption, and (c) selectivity to CO. Feed composition (v/v): 1% CO, 1% O_2, 60% H_2, and balance with He. SV = 60,000 cm^{-3} g^{-1} h^{-1}.

result of smaller particle size. With indiscernible of CuO to the CeO_2 support in the developed cluster structure, the close interaction was believed to enhance both the oxygen storage in the Ce^{3+}/Ce^{4+} redox couple and subsequently the CO-PROX in the Cu^{2+}/Cu^{3+} redox couple, and these cannot be seen as independent processes [12].

3.3. Selective CO Oxidation Activity. Following the results from the catalytic oxidation of the mixed oxides, the group with high activity (CuO loading of 20, 40, and 60 wt.%) was selected for further investigation on selective CO oxidation in H_2 rich stream. Plots of the CO conversion, O_2 consumption, and CO selectivity as functions of the reaction temperature are shown in Figures 5(a), 5(b), and 5(c), respectively. A significant lower CO conversion is clearly observed on the 60% CuO catalyst at low temperature. Though it was grouped with the catalyst of 20% and 40% CuO loading for CO oxidation, the lower specific area of the 60% CuO catalyst manifested its effects when 60% H_2 was introduced into the feed stream [10]. The 20% CuO catalyst performs the best in selective oxidation; it has over 95% of both the CO conversion and selectivity windows over the temperature range of 110–130°C.

The O_2 consumption in Figure 5(b) is similar to the 20% and 40% CuO catalysts, while the 60% CuO catalyst

shows about 20% lower of O_2 consumption throughout the temperature range, and the full consumption is reached only after 250°C. The selectivity to CO oxidation for the 40% and 60% CuO is ~65% and ~56%, respectively. The results from the characterization of the catalysts and selective CO oxidation suggested the higher hydrogen oxidation at low temperature for the catalyst with larger crystallite size of copper oxide [7, 18]. This is observed in Figure 5(c) with the lower the selectivity to CO oxidation for the 60% CuO at temperature lower than 130°C. Luo et al. [26] prepared CuO/CeO_2 by two different methods and showed that large crystallite sizes of CuO reduced the H_2-TPR reaction temperature. At high reaction temperatures (>130°C), the rate of hydrogen oxidation is increased, this in turn would lower the selectivity to CO oxidation, and these were observed in all CuO contents of the catalyst. This typical phenomenon is observed for CuO/CeO_2 catalysts [26, 28–31].

In addition, the catalytic activities of $CuO\text{-}CeO_2$ catalysts were related to their physical properties: crystallite sizes, morphology development of structures such as cluster, and agglomeration of particles and BET surface area. The catalysts had been identified to exist in a form of mixed crystallites of monoclinic CuO and cubic CeO_2 structures. At low CuO content (10–20 wt.%), CeO_2 support can effectively anchors and disperse CuO, and this result in a uniform morphology and narrow particle size distribution of copper species. The aggregation of nanoparticles generates voids and together with small CuO crystallite size of ~5.9 nm is responsible for the high specific surface area (~109.2 m^2/g) of the mixed oxides. As the content of CuO was increased, CuO began to form loosely packed CuO cluster structures (CuO content between 20 and 40 wt.%) and eventually the excess CuO aggregated and form bulk-like crystalline CuO (>40 wt.% CuO). Drastic reduction of BET surface area was seen in catalysts with high CuO content due to the formation of large bulk-like crystalline CuO. The agglomeration of crystallites into larger copper particles reduces the interface area and results in the weakening of the metal-support interaction. A reverse morphology, described as finely dispersed of ceria crystallites over a copper oxide support, occurred at the CuO content greater than 80 wt.%. The optimal CuO loading (between 10 and 20 wt.%) provides the catalysts with small crystallite sizes, high specific surface area, and the formation of small CuO cluster, identified by researchers [9, 16, 18] as the most active morphology for CO oxidation, had been evidenced in the results of our characterization studies of the catalysts. The catalyst with CuO loading of 20 wt.% performed best in selective CO oxidation in excess H_2 by achieving the full CO conversion and 100% selectivity at 120°C. The high activity of the catalysts at low temperatures is believed to be a result of strong interaction of the active metal with the support and the synergism between copper and cerium in the facile redox couples.

4. Conclusions

The CO poisoning of PEMFCs is a major problem to deplete the efficiency and energy conversion of PEMFCs. To remove a trace amount of CO in the reformed gas is essential. In this work, the catalytic performance of $CuO\text{-}CeO_2$ in selective CO oxidation in the presence of excess hydrogen has been studied. The content of CuO in the catalysts has strong affects to their physical properties and their catalytic activities to the reaction. High CO conversion at low temperature was obtained when the catalysts contained the small crystallite sizes, high specific surface area, and the formation of small CuO cluster. Under our catalyst preparation condition, we found that the optimal CuO content of $CuO\text{-}CeO_2$ catalysts using in CO-PROX was 20% with high CO conversion and high selectivity to CO oxidation over the temperature range of 110–130°C.

Acknowledgment

The authors gratefully acknowledge the financial support from Faculty of Engineering, Burapha University under the Contract no. 16/2550.

References

[1] E. Moretti, L. Storaro, A. Talon et al., "Effect of thermal treatments on the catalytic behaviour in the CO preferential oxidation of a $CuO\text{-}CeO_2\text{-}ZrO_2$ catalyst with a flower-like morphology," *Applied Catalysis B*, vol. 102, no. 3-4, pp. 627–637, 2011.

[2] J. Li, P. Zhu, S. Zuo, Q. Huang, and R. Zhou, "Influence of Mn doping on the performance of $CuO\text{-}CeO_2$ catalysts for selective oxidation of CO in hydrogen-rich streams," *Applied Catalysis A*, vol. 381, no. 1-2, pp. 261–266, 2010.

[3] M. Moreno, L. Bergamini, G. T. Baronetti, M. A. Laborde, and F. J. Mariño, "Mechanism of CO oxidation over CuO/CeO_2 catalysts," *International Journal of Hydrogen Energy*, vol. 35, no. 11, pp. 5918–5924, 2010.

[4] M. P. Woods, P. Gawade, B. Tan, and U. S. Ozkan, "Preferential oxidation of carbon monoxide on Co/CeO_2 nanoparticles," *Applied Catalysis B*, vol. 97, no. 1-2, pp. 28–35, 2010.

[5] N. K. Gamboa-Rosales, J. L. Ayastuy, M. P. González-Marcos, and M. A. Gutiérrez-Ortiz, "Effect of Au promoter in CuO/CeO_2 catalysts for the oxygen-assisted WGS reaction," *Catalysis Today*, vol. 176, no. 1, pp. 63–71, 2011.

[6] K.-S. Lin, S. Chowdhury, H.-P. Yeh, W.-T. Hong, and C.-T. Yeh, "Preparation and characterization of $CuO/ZnO\text{-}Al_2O_3$ catalyst washcoats with CeO_2 sols for autothermal reforming of methanol in a microreactor," *Catalysis Today*, vol. 164, no. 1, pp. 251–256, 2011.

[7] C. G. MacIel, L. P. R. Profeti, E. M. Assaf, and J. M. Assaf, "Hydrogen purification for fuel cell using $CuO/CeO_2\text{-}Al_2O_3$ catalyst," *Journal of Power Sources*, vol. 196, no. 2, pp. 747–753, 2011.

[8] C.-T. Peng, H. Lia, B. Liaw, and Y. Chen, "Removal of CO in excess hydrogen over $CuO/Ce_{1-x}Mn_xO$ catalysts," *Chemical Engineering Journal*, vol. 172, pp. 452–458, 2011.

[9] A. Razeghi, A. Khodadadi, H. Ziaei-Azad, and Y. Mortazavi, "Activity enhancement of Cu-doped ceria by reductive regeneration of $CuO\text{-}CeO_2$ catalyst for preferential oxidation of CO in H_2-rich streams," *Chemical Engineering Journal*, vol. 164, no. 1, pp. 214–220, 2010.

[10] S. S. Maluf, P. A. P. Nascente, and E. M. Assaf, "CuO and CuO-ZnO catalysts supported on CeO_2 and $CeO_2\text{-}LaO_3$ for low temperature water-gas shift reaction," *Fuel Processing Technology*, vol. 91, no. 11, pp. 1438–1445, 2010.

[11] S. Zeng, H. Su, Y. Liu, Y. Wang, and D. Wang, "CuO-CeO_2/Al_2O_3/FeCrAl monolithic catalysts prepared by in situ combustion synthesis method for preferential oxidation of carbon monoxide," *Journal of Rare Earths*, vol. 29, no. 1, pp. 69–73, 2011.

[12] A. L. Cámara, A. Kubacka, Z. Schay, Z. Koppány, and A. Martínez-Arias, "Influence of calcination temperature and atmosphere preparation parameters on CO-PROX activity of catalysts based on CeO_2/CuO inverse configurations," *Journal of Power Sources*, vol. 196, no. 9, pp. 4364–4369, 2011.

[13] A. Gurbani, J. L. Ayastuy, M. P. González-Marcos, and M. A. Gutiérrez-Ortiz, "CuO-CeO_2 catalysts synthesized by various methods: comparative study of redox properties," *International Journal of Hydrogen Energy*, vol. 35, no. 20, pp. 11582–11590, 2010.

[14] J. L. Ayastuy, N. K. Gamboa, M. P. González-Marcos, and M. A. Gutiérrez-Ortiz, "CuO/CeO_2 washcoated ceramic monoliths for CO-PROX reaction," *Chemical Engineering Journal*, vol. 171, no. 1, pp. 224–231, 2011.

[15] H. Zou, S. Chen, Z. Liu, and W. Lin, "Selective CO oxidation over CuO-CeO_2 catalysts doped with transition metal oxides," *Powder Technology*, vol. 207, no. 1–3, pp. 238–244, 2011.

[16] Z. Wu, H. Zhu, Z. Qin, H. Wang, L. Huang, and J. Wang, "Preferential oxidation of CO in H_2-rich stream over CuO/$Ce_{1-x}Ti_xO_2$ catalysts," *Applied Catalysis B*, vol. 98, pp. 204–212, 2010.

[17] J. L. Ayastuy, A. Gurbani, M. P. González-Marcos, and M. A. Gutiérrez-Ortiz, "Effect of copper loading on copper-ceria catalysts performance in CO selective oxidation for fuel cell applications," *International Journal of Hydrogen Energy*, vol. 35, no. 3, pp. 1232–1244, 2010.

[18] B. Qiao, A. Wang, J. Lin, L. Li, D. Su, and T. Zhang, "Highly effective CuO/$Fe(OH)_x$ catalysts for selective oxidation of CO in H_2-rich stream," *Applied Catalysis B*, vol. 105, no. 1-2, pp. 103–110, 2011.

[19] J. L. Ayastuy, A. Gurbani, M. P. González-Marcos, and M. A. Gutiérrez-Ortiz, "Selective CO oxidation in H_2 streams on CuO/$Ce_xZr_{1-x}O_2$ catalysts: correlation between activity and low temperature reducibility," *International Journal of Hydrogen Energy*, vol. 37, no. 2, pp. 1993–2006, 2012.

[20] G. Sun, X. Mu, Y. Zhang, Y. Cui, G. Xia, and Z. Chen, "Rare earth metal modified CuO/γ-Al_2O_3 catalysts in the CO oxidation," *Catalysis Communications*, vol. 12, pp. 349–352, 2011.

[21] J. L. Ayastuy, A. Gurbani, M. P. González-Marcos, and M. A. Gutiérrez-Ortiz, "CO oxidation on $Ce_xZr_{1-x}O_2$-supported CuO catalysts: correlation between activity and support composition," *Applied Catalysis A*, vol. 387, pp. 119–128, 2010.

[22] Z. Lendzion-Bielun, M. M. Bettahar, and S. Monteverdi, "Fe-promoted CuO/CeO_2 catalyst: structural characterization and CO oxidation activity," *Catalysis Communications*, vol. 11, no. 14, pp. 1137–1142, 2010.

[23] L. Li, L. Song, H. Wang et al., "Water-gas shift reaction over CuO/CeO_2 catalysts: effect of CeO_2 supports previously prepared by precipitation with different precipitants," *International Journal of Hydrogen Energy*, vol. 36, no. 15, pp. 8839–8849, 2011.

[24] B. Skårman, T. Nakayama, D. Grandjean et al., "Morphology and structure of CuO_x/CeO_2 nanocomposite catalysts produced by inert gas condensation: an HREM, EFTEM, XPS, and high-energy diffraction study," *Chemistry of Materials*, vol. 14, no. 9, pp. 3686–3699, 2002.

[25] M. Jobbagy, F. Mariño, B. Schönbrod, and G. Baronetti, "Synthesis of copper-promoted CeO_2 catalysts," *Chemistry of Materials*, vol. 18, pp. 1945–1950, 2006.

[26] M.-F. Luo, J.-M. Ma, J.-Q. Lu, Y.-P. Song, and Y.-J. Wang, "High-surface area CuO-CeO_2 catalysts prepared by a surfactant-templated method for low-temperature CO oxidation," *Journal of Catalysis*, vol. 246, pp. 52–59, 2007.

[27] Y. Liu, Q. Fu, and M. F. Stephanopoulos, "Preferential oxidation of CO in H_2 over CuO-CeO_2 catalysts," *Catalysis Today*, vol. 93–95, pp. 241–246, 2004.

[28] A. Gómez-Cortés, Y. Márquez, J. Arenas-Alatorre, and G. Díaz, "Selective CO oxidation in excess of H_2 over high-surface area CuO/CeO_2 catalysts," *Catalysis Today*, vol. 133–135, no. 1–4, pp. 743–749, 2008.

[29] Z. Liu, R. Zhou, and X. Zheng, "Comparative study of different methods of preparing CuO-CeO_2 catalysts for preferential oxidation of CO in excess hydrogen," *Journal of Molecular Catalysis A*, vol. 267, no. 1-2, pp. 137–142, 2007.

[30] P. K. Cheekatamarla, W. S. Epling, and A. M. Lane, "Selective low-temperature removal of carbon monoxide from hydrogen-rich fuels over Cu-Ce-Al catalysts," *Journal of Power Sources*, vol. 147, no. 1-2, pp. 178–183, 2005.

[31] L.-C. Chung and C.-T. Yeh, "Synthesis of highly active CuO-CeO_2 nanocomposites for preferential oxidation of carbon monoxide at low temperatures," *Catalysis Communications*, vol. 9, no. 5, pp. 670–674, 2008.